

# Benchmarks of Nonclassicality for Qubit Arrays

Mordecai Waegell<sup>1</sup> and Justin Dressel<sup>1,2</sup>

<sup>1</sup>*Institute for Quantum Studies, Chapman University, Orange, CA, USA*

<sup>2</sup>*Schmid College of Science and Technology, Chapman University, Orange, CA, USA\**

**Keywords:** Benchmark, Quantum Computing, Entanglement Witness, Bell Inequality, Quantum Circuits

arXiv:1812.07821v1 [quant-ph] 19 Dec 2018

---

\* Corresponding Author: dressel@chapman.edu; Keck Center for Science and Engineering, Chapman University, One University Drive, Orange, CA 92866;  
Phone: (714) 516-5949

**Abstract:** We present a set of practical benchmarks for qubit arrays that economically test the fidelity of achieving multi-qubit nonclassicality. The benchmarks are measurable correlators similar to 2-qubit Bell correlators, and are derived from a particular set of geometric structures from the  $N$ -qubit Pauli group for  $N = 3, \dots, 9$  qubits. These structures prove the Greenberger-Horne-Zeilinger (GHZ) theorem, while the derived correlators witness genuine  $N$ -partite entanglement and establish a tight lower bound on the fidelity of particular stabilizer state preparations. The correlators need only  $M \leq N + 1$  distinct measurement settings, as opposed to the  $2^{2N} - 1$  settings that would normally be required to tomographically verify their associated stabilizer states. We optimize the measurements of these correlators for a physical array of qubits that can be nearest-neighbor-coupled with controlled- $Z$  gates, and provide circuits with a constant gate depth for testing 3–9 qubits with linear cluster states. Since measuring a benchmark stabilizes its associated state, it is possible to periodically check the benchmark during a larger protocol requiring that stabilized state. We numerically simulate the provided circuits for a realistic scenario, using ranges of  $T_1$  energy relaxation times,  $T_2$  dephasing times, and controlled- $Z$  gate-fidelities consistent with Google’s 9-qubit superconducting chip. The simulations verify the tightness of the fidelity bounds and witness nonclassicality for all nine qubits, while also showing ample room for improvement in chip performance.

## INTRODUCTION

As hardware is developed to implement quantum circuits on increasing numbers of qubits, it will be valuable to have economical benchmarks of fully quantum behavior. From the outset of quantum computing it has been clear that the advantage of a quantum computer lies somewhere in its ability to readily perform tasks that are physically challenging or impossible for a classical system. Therefore, ideal benchmarks should certify the presence of such nonclassical behavior. Despite this broad intuition, identifying and quantifying the specific nonclassical resources that lead to quantum computational advantage has remained an elusive goal [1], with several earlier proposals for suitable measures like entanglement [2–5], Bell-nonlocality [6–11], or quantum discord and its variations [12–14], proving to be insufficient on their own due to the discovery of algorithmic counter-examples [15–19]. Recent advances also suggest a strong connection between quantum advantage and contextuality [20–24], which is a general structural feature of quantum mechanics that subsumes nonlocality. The most accepted metric of nonclassical behavior in quantum devices, however, is the violation of two-qubit Bell inequalities.

In this article we provide a set of practical nonclassicality benchmarks that naturally generalize two-qubit Bell inequality tests to  $N = 3, \dots, 9$  qubits, based on the Greenberger-Horne-Zeilinger (GHZ) theorem. As with Bell inequalities, our benchmarks use the experimental violation of a classical bound to characterize the nonclassical behavior of the circuit. These benchmarks are optimized for qubit arrays with nearest-neighbor coupling. We provide efficient circuits for implementing these benchmarks with controlled- $Z$  entangling gates, with a constant gate depth of 4 (up to hardware-specific decompositions of the controlled- $Z$  gate [25–30]). Measuring these benchmarks produces a tight lower bound on the fidelity with which a particular stabilizer state or stabilizer subspace has been prepared. These benchmarks generalize earlier work which was experimentally tested with  $N = 3, 4$  photons [31].

## RESULTS

*Nonclassicality Benchmarks:*— Our benchmarks consist of measurable correlators that are compared to derived upper bounds; violation of these bounds characterizes nonclassicality. Each such benchmark corresponds to a specific prepare-and-measure circuit on  $N$ -qubits with  $M \leq N + 1$  different measurement settings. The  $M$  observables form a structure called an ID (also called an *identity product* [32]), which is a set of mutually commuting  $N$ -qubit Pauli operators whose overall product is the  $N$ -qubit identity, up to a sign. We express an ID as an  $M \times N$  table of single-qubit Pauli operators and the identity  $\{Z, X, Y, I\}$ , labeled  $O_{ij}$  with  $i = 1, \dots, M$  and  $j = 1, \dots, N$ . We also define the shortened label  $O_i = \bigotimes_{j=1}^N O_{ij}$  to indicate the  $N$ -qubit observable obtained as the product of the  $i$ th row of an ID. We omit tensor product symbols for compactness.

To obtain the Bell inequality for each ID [31], we choose a particular eigenspace  $\Pi$  represented by a projector of rank  $2^{N-M+1}$ , which is specified by the set of  $N$ -qubit Pauli observables  $\{O_i\}$  that form the  $M$  rows of the ID (see Fig. 1), and a specific choice of their respective eigenvalues  $\{\lambda_i\}$ . We then define the *correlator* observable for this chosen eigenspace,

$$\alpha = \sum_{i=1}^M \lambda_i O_i, \quad (1)$$

such that its expectation value in a state  $\rho$  has an upper bound of  $\beta_{QM} = M$ , saturated by the chosen eigenspace  $\rho = \Pi$ ,

$$\langle \alpha \rangle = \sum_{i=1}^M \lambda_i \text{Tr}(\rho O_i) \leq \beta_{QM} = M. \quad (2)$$

For example, we could prepare the joint eigenstate of the ID of Fig. 1(a), with negative eigenvalue  $\lambda_1 = -1$  for the 3-qubit Pauli observable  $O_1 = YXY$ , and positive eigenvalues  $\lambda_2 = \lambda_3 = \lambda_4 = +1$  for the remaining observables  $O_2 = YYZ$ ,  $O_3 = ZXZ$ , and  $O_4 = ZYY$ . Then,  $\langle \alpha \rangle = \text{Tr}(\Pi \alpha) = 4$  since each term in the sum becomes  $+1$ .

In the spirit of Bell [7, 8], if one tries to explain the observed correlation by choosing a complete set of local hidden variables  $v_{Zj}, v_{Xj}, v_{Yj} \in \{+1, -1\}$  that predict the outcomes of the single-qubit Pauli measurements, then at least one of the terms in the correlator sum becomes  $-1$ , resulting in a smaller upper bound,

$$\langle \alpha \rangle \leq \beta_{\text{LHVT}} = M - 2. \quad (3)$$

Experimental violation of this bound thus indicates nonclassicality in the form of a violation of local realism. Though the locality loophole is always open for neighboring qubits on a chip, this violation is still a useful witness for nonclassical states prepared by the chip, much like for Bell inequalities or Bell-Leggett-Garg inequalities [33]. The derivation of this bound is reviewed in the Methods Section.

As an independent result, maximizing the expectation value of the correlator over all biseparable quantum states in the  $N$ -qubit Hilbert space produces the upper bound,

$$\langle \alpha \rangle \leq \beta_{\text{bisep}} = M - 2, \quad (4)$$

which happens to coincide with the bound for local hidden variable theories. Experimental violation of the bound thus also witnesses genuine  $N$ -partite entanglement. In the Methods section, we provide the proof that the joint eigenspaces of the IDs in this article are maximally entangled, as well as the derivation of this bound.

In light of the convenient fact that  $\beta_{\text{bisep}} = \beta_{\text{LHVT}}$ , we define the *nonclassicality benchmark score* for a given physical  $N$ -qubit device as the experimentally determined value,

$$\mathcal{B} = \frac{\langle \alpha \rangle_{\text{exp}} - M + 2}{2}, \quad (5)$$

such that  $\mathcal{B} \leq 0$  fails to witness either entanglement or the violation of local realism, while  $0 < \mathcal{B} \leq 1$  witnesses nonlocal  $N$ -partite-entangled states. The nonclassicality benchmark score thus serves as a metric of uniquely quantum behavior, with  $\mathcal{B} = 1$  indicating maximum nonclassicality that saturates the correlator bound. Each  $N$ -qubit ID provides a benchmark corresponding to a distinct nonclassical eigenspace of an  $N$ -qubit physical device, and thus the hierarchy of IDs presented in Fig. 1 provides a corresponding hierarchy of benchmarks.

*Lower Bounding the Fidelity:*— The correlator also serves to bound the fidelity from below [31],

$$F \geq F_{\text{ID}} = \frac{\langle \alpha \rangle_{\text{exp}} - M + 4}{4} = \frac{\mathcal{B} + 1}{2}, \quad (6)$$

where  $F = \text{Tr}(\rho_{\text{exp}}\Pi) \in [0, 1]$  is the fidelity that the experimentally prepared state  $\rho_{\text{exp}}$  lies within the eigenspace  $\Pi$  stabilized by the chosen ID. We provide a general derivation of this bound in the Methods section. Importantly, in the limit  $\langle \alpha \rangle_{\text{exp}} \rightarrow \beta_{\text{QM}} = M$ , we have  $F_{\text{ID}} \rightarrow 1$ , and thus as the fidelity of the preparation is improved, this lower bound obviates the need for full tomography of these preparations.

Taken together, the inequalities of Eqs. 3, 4, and 6 provide a practical and efficient characterization of the prepared  $N$ -qubit state, as well as a robust benchmark of its nonclassical behavior, using only  $M \leq N + 1$  measurement settings. Since these measurement settings mutually commute by construction, this characterization could also be implemented within a larger stabilizer-based protocol using quantum nondemolition measurements.

*Benchmark Circuits and Simulation:*— The IDs in this article have been specially chosen so that the prepare-and-measure circuit for each measurement setting requires a gate depth of 4 on any array of  $N$  physical qubits with only nearest-neighbor controlled- $Z$  couplings, making them a scalable and uniform set of benchmarks for implementations of this type. Figure 2 shows the circuits for  $N = 4, 5$ , from which the generalization to all  $N$  should be straightforward. In general, each circuit prepares an  $N$ -qubit linear cluster state, which is contained within the maximally entangled subspace of the corresponding ID.

In order to evaluate the usefulness of these benchmarks in real-world physical implementations, we simulated the performance of these circuits for each of the IDs in Fig. 1. We simulated each circuit over a range of  $T_1$  energy relaxation times,  $T_2$  dephasing times, and angular jitter for the controlled- $Z$  gate rotations, using the ranges given in Figs. 3 and 4. We also considered the effect of initialization and readout error for each qubit. The ranges of values were chosen to match the reported values of the 9-qubit Google chip [28, 29], with the experimental values roughly in the center of each simulated range. We ran one version of the simulation using a nominal initialization error for each qubit of  $P_e = 2\%$ , and another version where we used the observed initialization errors for each of the nine qubits on the Google chip. Final readout error has been neglected as correctable for ensemble statistics. Selected plots from the simulations are shown in Fig. 3, while scatter plots of the lower fidelity bound,  $F_{\text{ID}}$ , are shown in Fig. 4 for the full ranges of simulated values. Note that in order to minimize the effect of the two worst qubits on the chip (boldface values in Figs. 3 and 4), we always used the last  $N$  qubits on the chip to form our  $N$ -qubit IDs in the simulation. See the Methods section for additional details about how the numerical simulations were performed.

Judging by our simulated data shown in Figs. 3 and 4, we expect the 9-qubit Google chip to be able to violate the classicality bounds for all nine qubits. We can see clearly that the qubit initialization error is the dominant source of error as we try to move to larger  $N$ . This shows that our benchmarking scheme is immediately relevant, since it appears that similar hardware fidelity would only violate the bound for one or two more qubits — but certainly not all 72 on the Bristlecone chip [34] —

once suitable IDs have been found beyond the 9 presented here.

## DISCUSSION

The IDs and implementation circuits presented in this article are good benchmark tests for any physical implementation of qubits in a nearest-neighbor-connected array. They work naturally on a chip with more connectivity than this as well. While our simulations targeted a particular recent chip implementation for concreteness, this does not constrain the general usefulness of this protocol for other multi-qubit systems.

Although some families of IDs with the same properties as those in Fig. 1 are known for all  $N$  [32, 35], the IDs with the smallest possible value of  $M$  for a given  $N$  are not known in general. Because of their geometric nature, enumerating all of the representative IDs for given values of  $N$  and  $M$  is a highly nontrivial problem, related to solving the graph isomorphism problem on  $N \times M$  colored vertices, and it is thus limited by computational resources. Furthermore, not every ID can be constructed using only nearest-neighbor couplings in linear circuits as in Fig. 2. The increased connectivity of more modern chips, like the Bristlecone chip from Google, should allow the use of more general IDs, although the circuit depth will likely increase by one or two gates. At present, we have examples of maximally entangled IDs which prove the GHZ theorem for  $N = 10$ ,  $M = 6$ , and  $N = 11$ ,  $M = 7$ , but we have not yet optimized the circuits for nearest-neighbor coupling; beyond this, IDs with minimal  $M$  are not known.

Each of the IDs presented here also gives rise to a complete proof of the Kochen-Specker (KS) theorem for contextuality [20, 36, 37], which can be implemented for any initial state with a few alternative circuits for the different measurement contexts. In general, IDs are the natural building blocks of proofs of the KS theorem in the  $N$ -qubit Pauli group. This is a slightly more complicated setup, which could inspire different contextuality-based benchmarks in future work.

Finally, maximally entangled IDs with  $M < N + 1$  give rise to maximally entangled eigenspaces, each of dimension  $2^{N-M+1}$ , which generalize the codespaces of error correcting codes [38, 39], and  $L = N - M + 1$  is the number of *logical qubits* (where  $N$  is the number of *physical qubits*). All  $N$ -qubit-stabilizer-based error correcting codes (including the toric code [40]) belong to the family of IDs, but not all IDs can be used to diagnose the syndrome of an error. Many of the well-known error correcting codes generate an ID which proves the GHZ theorem, and all can be used as entanglement witnesses in the manner of this article [41]. Nevertheless, these more general maximally entangled subspaces may be of significant interest for other applications in quantum information processing, which warrants further investigation. One straightforward application for these subspaces is to perform benchmarks that measure physical qubits as described in this paper, while simultaneously benchmarking the performance of the logical qubits in some additional way. The two tests may be performed simultaneously because any general logical  $L$ -qubit state can be prepared for each benchmark, although the circuit is likely to be longer and more complex than Fig. 2, and the performance will be commensurately worse.

## METHODS

*Proving the GHZ Theorem:* All of the IDs in Fig. 1 have sign -1, and for each qubit  $j$ , the number of entries  $O_{ij} = Z$  in the ID is even, as is the number of entries with  $O_{ij} = X$  and with  $O_{ij} = Y$ . These properties indicate that these IDs give rise to proofs of the GHZ theorem [9], which is a logical version of Bell's nonlocality theorem [7, 8], without any

inequalities. To see this, suppose that a joint eigenstate (i.e., any state in a joint eigenspace) of these observables is prepared. This eigenstate has  $M$  eigenvalues  $\lambda_i$  corresponding to the  $M$  observables, and  $\prod_{i=1}^M \lambda_i = -1$ , since the product of these  $M$  observables is  $-I^{\otimes N}$ . Suppose that each of the  $N$  qubits are now mutually space-like separated, and each is subjected to random local Pauli measurements, and label their outcomes  $\lambda_{ij}$ , when all  $N$  local measurement settings happen to correspond to observable  $i$  of the ID. The entanglement correlations that are obeyed by this state are  $\prod_{j=1}^N \lambda_{ij} = \lambda_i$ . Putting these relations together we have  $\prod_{i=1}^M \prod_{j=1}^N \lambda_{ij} = -1$ . Now, in order for a local hidden variable theory (LHVT) to explain these entanglement correlations, each qubit  $j$  must carry local hidden variables  $v_{Zj}, v_{Xj}, v_{Yj} \in \{+1, -1\}$  which predict the outcomes  $\lambda_{ij}$ , and are pre-arranged to satisfy the entanglement constraints. However, for such hidden variables we would have  $\prod_{i=1}^M \prod_{j=1}^N \lambda_{ij} = \prod_{j=1}^N v_{Zj}^{n_j} v_{Xj}^{m_j} v_{Yj}^{l_j} = +1$ , since  $n_j, m_j$ , and  $l_j$  are all even for the IDs of this article, and thus it is impossible to choose local hidden variables which can satisfy the entanglement correlations of this state. This logical proof without inequalities can be converted into a Bell inequality for use as a benchmark of  $N$ -qubit nonlocality, as shown in the main text, by noting that for any complete assignment of local hidden variables  $v_{Zj}, v_{Xj}, v_{Yj} \in \{+1, -1\}$  to the ID, at least one of the observables has the wrong eigenvalue.

In general, proving the GHZ theorem does not prove that nonlocal correlations exist between more than just a single pair of qubits among the  $N$  [42–45], however the IDs of this article are also chosen to be  $N$ -partite entanglement witnesses [46, 47], such that the Bell inequality can only be violated by a genuinely  $N$ -qubit-entangled state. Violation of the corresponding Svetlichny inequalities overcomes this limitation [48], proving that nonlocal correlations exist between every pair of qubits among the  $N$ , but the set of observables that must be measured no longer mutually commute, and only the Bell inequality form of the argument works. Our method circumvents this limitation in a different way, by proving that only a maximally entangled  $N$ -qubit state can violate the bound. Monogamy of entanglement can then be logically extended to monogamy of nonlocal correlations.

*Bounding the Fidelity:* An  $N$ -qubit ID with  $M$  observables  $\{O_i\}$  has a complete set of eigenspaces  $\{\Pi_k\}$  satisfying  $\sum_k \Pi_k = I$ , each of which can be identified by a unique set of distinct eigenvalues  $\{\lambda_{ik}\}$  of  $\{O_i\}$ . Only  $M - 1$  of the observables in an ID are independent, and if  $M - 1 < N$  the eigenspaces  $\Pi_k$  are degenerate, and each contains  $2^{N-M+1}$  mutually orthogonal vectors  $|\kappa_{jk}\rangle$  which share the eigenvalue  $\lambda_{ik}$ , with  $j = 1, \dots, 2^{N-M+1}$ , such that  $\{|\kappa_{jk}\rangle\}$  is a complete orthonormal eigenbasis of the ID. Each of the  $2^{M-1}$  eigenspaces  $\Pi_k$  corresponds to a unique correlator  $\alpha_k = \sum_{i=1}^M \lambda_{ik} O_i$ . Each experimentally obtained quantity  $\langle \alpha_k \rangle$  enables us to put a lower bound on the fidelity that an experimentally prepared pure state  $|\psi\rangle$  lies within the eigenspace  $\Pi_k$  [31].

With no loss of generality, we will henceforth use correlator  $\alpha_1$  and the target eigenspace  $\Pi_1$ . We begin by expanding  $|\psi\rangle$  in this eigenbasis as,

$$|\psi\rangle = \sum_{j=1}^{2^{N-M+1}} \left[ a_j |\kappa_{j1}\rangle + \sum_{k=2}^{M-1} b_{jk} |\kappa_{jk}\rangle \right], \quad (7)$$

such that  $\sum_j (|a_j|^2 + \sum_{k=2}^{M-1} |b_{jk}|^2) = 1$ .

Since the expansion is in an eigenbasis of  $\alpha_1$ , we find

$$\langle \alpha_1 \rangle_{\text{exp}} = \langle \psi | \alpha_1 | \psi \rangle = \sum_{j=1}^{2^{N-M+1}} \left[ |a_j|^2 \langle \kappa_{j1} | \alpha_1 | \kappa_{j1} \rangle + \sum_{k=2}^{M-1} |b_{jk}|^2 \langle \kappa_{jk} | \alpha_1 | \kappa_{jk} \rangle \right]. \quad (8)$$

Note that  $\langle \kappa_{j1} | \alpha_1 | \kappa_{j1} \rangle = \sum_{k=1}^M \lambda_k^2 = M$ , since all eigenvalues of  $|\kappa_1\rangle$  match those in the correlator  $\alpha_1$  by construction, and thus square to 1. However, any other  $|\kappa_{jk}\rangle$  does not lie within  $\Pi_1$ , so is characterized by eigenvalues distinct from those characterizing  $\Pi_1$ . Moreover, since the product of all eigenvalues for the observables of a given ID is fixed for any eigenstate, only even numbers of eigenvalues can differ from those characterizing  $\Pi_1$ , which necessarily causes at least two terms of  $\langle \kappa_{jk} | \alpha_1 | \kappa_{jk} \rangle$  to become  $-1$ , resulting in an upper bound of  $\langle \kappa_{jk} | \alpha_1 | \kappa_{jk} \rangle \leq M - 4$  for those eigenstates. Using these two observations we obtain,

$$\langle \alpha_1 \rangle_{\text{exp}} \leq \sum_{j=1}^{2^{N-M+1}} \left[ |a_j|^2 M + \sum_{k=2}^{2^{M-1}} |b_{jk}|^2 (M-4) \right] = 4F + M - 4, \quad (9)$$

where  $F = \sum_j |a_j|^2$ , and we have used  $\sum_j (|a_j|^2 + \sum_{k=2}^{2^{M-1}} |b_{jk}|^2) = 1$ . We can rewrite this relation as

$$F \equiv \langle \psi | \Pi_1 | \psi \rangle \geq \frac{\langle \alpha_1 \rangle_{\text{exp}} - M + 4}{4} \equiv F_{\text{ID}}. \quad (10)$$

Noting that the left hand side of this equation is the fidelity  $F$  for the preparation  $|\psi\rangle$  to lie within the eigenspace  $\Pi_1$ , the right hand side  $F_{\text{ID}}$  gives a lower bound  $F \geq F_{\text{ID}}$  for the fidelity. For IDs with  $M = N + 1$ , the target subspace  $\Pi_1$  contains only one eigenvector, so the fidelity  $F$  is also a state preparation fidelity for the particular target eigenstate  $|\kappa_1\rangle$ . For IDs with  $M < N + 1$ , the target subspace  $\Pi_1$  is degenerate, so the fidelity  $F$  is the fidelity for  $|\psi\rangle$  to lie within that subspace.

Next we generalize the above derivation to the case of mixed states. For a general convex combination of  $m$  pure states,

$$\rho = \sum_{j=1}^m c_l |\psi_l\rangle \langle \psi_l|, \quad (11)$$

where  $\sum c_l = 1$ , we can expand each  $|\psi_l\rangle$  using appropriate eigenbases of the ID as in Eq. (7) and follow the same arguments to obtain

$$\langle \alpha_1 \rangle_{\text{exp}} \leq \sum_{l=1}^m c_l (4F_l + M - 4), \quad (12)$$

where  $F_l \equiv \langle \psi_l | \Pi_1 | \psi_l \rangle$ . We can rewrite this as,

$$F \equiv \text{Tr}(\rho \Pi_1) = \sum_{j=1}^m c_l F_l \geq \frac{\langle \alpha_1 \rangle_{\text{exp}} - M + 4}{4} \equiv F_{\text{ID}}. \quad (13)$$

As in the pure state case, the left hand side is the fidelity  $F$  for the mixed state  $\rho$  to lie within the target subspace  $\Pi_1$ , while the same expression for the right hand side  $F_{\text{ID}}$  places a lower bound on this fidelity.

*Witnessing Genuine N-Partite Entanglement:* An  $N$ -qubit ID provides an entanglement witness if it is maximally entangled [32, 49]. Entanglement is usually discussed in reference to the separability of states. However, there is a way to reason about the entanglement of a set of observables directly without reference to states. We define a maximally entangled set of  $N$ -qubit observables as one with the property that there exists no bipartition of the  $N$  qubits into subsets of  $R$  and  $N - R$ , such that all of the observables in each subset  $\otimes_{k \in [1, R]} O_{ik}$  mutually commute. It follows from this definition that the joint eigenstates of this set are maximally entangled  $N$ -qubit stabilizer states.

To see this, consider that every stabilizer state (space) of  $N$  qubits has a stabilizer group of  $b = 2^g$  mutually commuting Pauli observables  $\{S_i\}$  and corresponding eigenvalues  $\{\lambda_i\}$ , and its density operator can be written as,

$$\rho = \frac{1}{d} \sum_{i=1}^b \lambda_i S_i, \quad (14)$$

where  $g$  is the number of independent generators in the set, and  $d = 2^N$  is the dimension of the Hilbert space. Note that if  $g < N$ , then  $\rho$  projects onto a subspace of rank  $r = 2^{N-g} > 1$ , and that  $g = M - 1$  for a minimal ID, which is just a specific subset of one or more complete stabilizer groups. If a stabilizer state is the tensor product of two smaller stabilizer states on subsystems  $A$  and  $B$ , it follows that its density operator can be written as,

$$\rho_{AB} = \left( \frac{1}{d^A} \sum_{i=1}^{b^A} \lambda_i^A S_i^A \right) \otimes \left( \frac{1}{d^B} \sum_{j=1}^{b^B} \lambda_j^B S_j^B \right) = \frac{1}{d^{AB}} \sum_{k=1}^{b^{AB}} \lambda_k^{AB} S_k^{AB}. \quad (15)$$

For the bipartition of the system into  $A$  and  $B$ , all of the stabilizer operators  $S_i^A = \otimes_{k \in A} O_{ik}$  mutually commute by definition. It follows that one can find such a mutually commuting bipartition for any separable state, and therefore if no such bipartition exists, then the set of observables is maximally entangled. All of the IDs presented in this article are maximally entangled in this way, which results in a witness inequality with the same bound as the Bell inequality.

All states within a maximally entangled eigenspace of an ID are maximally entangled, meaning that for all of them, the maximum squared-Schmid-coefficient across all bipartitions is  $1/2$ . For such an eigenstate  $|\psi\rangle$ , a standard entanglement witness is  $\mathcal{W} = \mathbb{1}/2 - |\psi\rangle\langle\psi|$ , and an experimental measurement of  $\langle\mathcal{W}\rangle < 0$  is a witness of genuine  $N$ -partite entanglement [47]. Noting that a superposition state  $a|\psi\rangle + b|\psi_\perp\rangle$  can only violate this bound for  $F = |a|^2 > 1/2$ , we obtain  $F_{\text{ID}} \leq F \leq 1/2$  for all biseparable states. Plugging this into  $F_{\text{ID}} = (\langle\alpha\rangle_{\text{exp}} - M + 4)/4$  yields  $\langle\alpha\rangle_{\text{bisep}} \leq M - 2$ , which is Eq. (4).

*Numerical Simulation Details:* In the simulation, the state is first degraded by initialization error. That is, ideally the  $N$  qubits are prepared in an initial ground state  $\otimes_{i=1}^N |0\rangle$ . However, each qubit has an error probability  $P_e^{(i)}$  of being initially excited, which produces a mixed initial bit state  $(1 - P_e^{(i)})|0\rangle\langle 0| + P_e^{(i)}|1\rangle\langle 1| = (1 - 2P_e^{(i)})|0\rangle\langle 0| + P_e^{(i)}I$ , and thus a degraded initial state  $\rho = \otimes_{i=1}^n [(1 - 2P_e^{(i)})|0\rangle\langle 0| + P_e^{(i)}I]$  with ground state fidelity  $\prod_{i=1}^n (1 - 2P_e^{(i)})$ . The final readout error for an ensemble average can be corrected if the readout misidentification probabilities  $P_e^i$  are known, and thus we have neglected the role of the readout error.

Each gate in Fig. 2 is then applied to the initial state  $\rho$ . For the Hadamard gate, it is sufficient to use a  $Y_{90}$  rotation,  $\exp(-iY\pi/4)$ . We decompose the controlled- $Z$  gate into an implementable  $ZZ_{90}$  entangling gate and single-qubit corrections:  $\exp(i\pi/4)[\exp(iZ\pi/4) \otimes \exp(iZ\pi/4)]\exp(-iZZ\pi/4)$ . We degraded each gate by  $T_1$  energy relaxation and  $T_2$  dephasing processes for the corresponding gate times  $\Delta t$ . For the energy relaxation time  $T_1$ , the first-order corrections for each individual qubit are accumulated and then applied to  $\rho$ . For each qubit  $\Delta\rho_i = (a_i^\dagger \rho a_i - \frac{1}{2}\{\rho, a_i^\dagger a_i\})\Delta t/T_1^i$ , where  $a_i$  is the lowering operator of the  $i$ th qubit tensored with identity for the other qubits, and  $\rho \rightarrow \rho + \sum_i \Delta\rho_i$ . This linear-order Lindblad-form update is sufficient since  $\Delta t/T_1^i \ll 1$ . For the dephasing time  $T_2$ , we directly construct the matrix,

$$D = \left( \begin{array}{cc} 1 & e^{-\Delta t/T_2} \\ e^{-\Delta t/T_2} & 1 \end{array} \right)^{\otimes N}, \quad (16)$$

for efficiency and apply gate dephasing using element-wise multiplication (MATLAB syntax `.*`), as  $\rho \rightarrow \rho .* D$ .

For simulating gate infidelity, we assume that the single-qubit gate fidelities are high enough for their errors to be neglected, and so simulate only a range of fidelities for the 2-qubit controlled- $Z$  gates. As a crude model for infidelity of a controlled- $Z$  gate, we add a random angular jitter  $\delta\varphi$  only to the  $ZZ$  rotation step,  $\exp[-iZZ(\pi/2 + \delta\varphi)/2]$ , and average over the effect of this jitter using a raised cosine distribution with a width  $w$ ,  $dP(\delta\varphi) = d(\delta\varphi)[1 + \cos(\pi\delta\varphi/w)]/(2w)$ , where  $\delta\varphi \in [-w, w]$  has compact angular support. This yields the averaged state update,

$$\rho \rightarrow \int e^{-i\zeta_i(\pi/2+\delta\varphi)/2} \rho e^{i\zeta_i(\pi/2+\delta\varphi)/2} dP(\delta\varphi) = \frac{1}{2} \left[ \rho + \zeta_i \rho \zeta_i + i(\zeta_i \rho - \rho \zeta_i) \left( \frac{\sin w}{w} - \frac{\sin w}{2(w+\pi)} - \frac{\sin w}{2(w-\pi)} \right) \right], \quad (17)$$

where  $\zeta_i$  is the tensor product of Pauli  $Z$  for the two qubits the controlled- $Z$  is acting on, and identity for all of the other qubits. The limit as  $w \rightarrow 0$  restores the unperturbed gate. This crude error model includes only one possible physical mechanism of infidelity for the controlled- $Z$  gate, but gives an indication of the gate sensitivity to imprecise angular control. Since the initialization error dominates the infidelity, the effect of the angular jitter is small.

**Acknowledgments:** We thank Josh Mutus and Daniel Sank for helpful commentary, as well as Eric Freda for helping to create some of the figures in this paper.

**Competing Interests:** There are no competing interests.

**Contributions:** MW developed the IDs for the benchmarks in this article, developed the benchmark inequalities, coded the simulations, and wrote the manuscript. JD developed the theory for the simulations, and co-wrote the manuscript.

**Funding:** MW was partially supported by the Fetzer Franklin Fund of the John E. Fetzer Memorial Trust. JD was partially supported by the Army Research Office (ARO) grant No. W911NF-15-1-0496, as well as No. W911NF-18-1-0178.

- 
- [1] V. Vedral, “The elusive source of quantum speedup,” *Foundations of Physics*, vol. 40, no. 8, pp. 1141–1154, 2010.
- [2] S. Hill and W. K. Wootters, “Entanglement of a pair of quantum bits,” *Physical Review Letters*, vol. 78, no. 26, p. 5022, 1997.
- [3] W. K. Wootters, “Entanglement of formation of an arbitrary state of two qubits,” *Physical Review Letters*, vol. 80, no. 10, p. 2245, 1998.
- [4] W. K. Wootters, “Entanglement of formation and concurrence,” *Quantum Information & Computation*, vol. 1, no. 1, pp. 27–44, 2001.
- [5] A. Wong and N. Christensen, “Potential multiparticle entanglement measure,” *Physical Review A*, vol. 63, no. 4, p. 044301, 2001.
- [6] A. Einstein, B. Podolsky, and N. Rosen, “Can quantum-mechanical description of physical reality be considered complete?,” *Physical Review*, vol. 47, no. 10, p. 777, 1935.
- [7] J. Bell, “On the Einstein-Podolsky-Rosen paradox,” *Physics*, vol. 1, no. 3, pp. 195–200, 1964.
- [8] J. Bell, “On the problem of hidden variables in quantum mechanics,” *Reviews of Modern Physics*, vol. 38, no. 3, pp. 447–452, 1966.
- [9] D. M. Greenberger, M. A. Horne, and A. Zeilinger, “Going beyond Bell’s theorem,” in *Bell’s theorem, quantum theory and conceptions of the universe*, pp. 69–72, Springer, 1989.
- [10] D. M. Greenberger, M. A. Horne, A. Shimony, and A. Zeilinger, “Bell’s theorem without inequalities,” *American Journal of Physics*, vol. 58, no. 12, pp. 1131–1143, 1990.
- [11] S. Bravyi, D. Gosset, and R. König, “Quantum advantage with shallow circuits,” *Science*, vol. 362, no. 6412, pp. 308–311, 2018.
- [12] B. Lanyon, M. Barbieri, M. Almeida, and A. White, “Experimental quantum computing without entanglement,” *Physical Review Letters*, vol. 101, no. 20, p. 200501, 2008.
- [13] A. Ferraro, L. Aolita, D. Cavalcanti, F. Cucchietti, and A. Acin, “Almost all quantum states have nonclassical correlations,” *Physical Review A*, vol. 81, no. 5, p. 052318, 2010.
- [14] K. Modi, A. Brodutch, H. Cable, T. Paterek, and V. Vedral, “The classical-quantum boundary for correlations: Discord and related measures,” *Reviews of Modern Physics*, vol. 84, pp. 1655–1707, Nov 2012.
- [15] C. H. Bennett, D. P. DiVincenzo, T. Mor, P. W. Shor, J. A. Smolin, and B. M. Terhal, “Unextendible product bases and bound entanglement,” *Physical Review Letters*, vol. 82, pp. 5385–5388, Jun 1999.
- [16] C. H. Bennett, D. P. DiVincenzo, C. A. Fuchs, T. Mor, E. Rains, P. W. Shor, J. A. Smolin, and W. K. Wootters, “Quantum nonlocality without entanglement,” *Physical Review A*, vol. 59, pp. 1070–1091, Feb 1999.
- [17] D. A. Meyer, “Sophisticated quantum search without entanglement,” *Physical Review Letters*, vol. 85, pp. 2014–2017, Aug 2000.
- [18] B. Dakić, V. Vedral, and Č. Brukner, “Necessary and sufficient condition for nonzero quantum discord,” *Physical Review Letters*, vol. 105, no. 19, p. 190502, 2010.

- [19] A. Bera, T. Das, D. Sadhukhan, S. S. Roy, A. S. De, and U. Sen, “Quantum discord and its allies: a review of recent progress,” *Reports on Progress in Physics*, vol. 81, no. 2, p. 024001, 2017.
- [20] S. Kochen and E. Specker, “The problem of hidden variables in quantum mechanics,” *J. of Math. and Mech.*, vol. 17, pp. 59–87, 1967.
- [21] E. F. Galvao, “Discrete Wigner functions and quantum computational speedup,” *Physical Review A*, vol. 71, no. 4, p. 042302, 2005.
- [22] M. Howard, J. Wallman, V. Veitch, and J. Emerson, “Contextuality supplies the ‘magic’ for quantum computation,” *Nature*, vol. 510, no. 7505, p. 351, 2014.
- [23] E. P. Wigner, “On hidden variables and quantum mechanical probabilities,” *American Journal of Physics*, vol. 38, no. 8, pp. 1005–1009, 1970.
- [24] A. A. Klyachko, M. A. Can, S. Binicioğlu, and A. S. Shumovsky, “Simple test for hidden variables in spin-1 systems,” *Physical Review Letters*, vol. 101, no. 2, p. 020403, 2008.
- [25] J. M. Chow, A. D. Córcoles, J. M. Gambetta, C. Rigetti, B. R. Johnson, J. A. Smolin, J. R. Rozen, G. A. Keefe, M. B. Rothwell, M. B. Ketchen, and M. Steffen, “Simple all-microwave entangling gate for fixed-frequency superconducting qubits,” *Physical Review Letters*, vol. 107, no. 8, p. 080502, 2011.
- [26] J. Ghosh, A. Galiutdinov, Z. Zhou, A. N. Korotkov, J. M. Martinis, and M. R. Geller, “High-fidelity controlled- $\sigma$  z gate for resonator-based superconducting quantum computers,” *Physical Review A*, vol. 87, no. 2, p. 022309, 2013.
- [27] J. M. Martinis and M. R. Geller, “Fast adiabatic qubit gates using only  $\sigma$  z control,” *Physical Review A*, vol. 90, no. 2, p. 022307, 2014.
- [28] R. Barends, J. Kelly, A. Megrant, A. Veitia, D. Sank, E. Jeffrey, T. C. White, J. Mutus, A. G. Fowler, B. Campbell, Y. Chen, Z. Chen, B. Chiaro, A. Dunsworth, C. Neill, P. O’Malley, P. Roushan, A. Vainsencher, J. Wenner, A. N. Korotkov, A. N. Cleland, and J. M. Martinis, “Superconducting quantum circuits at the surface code threshold for fault tolerance,” *Nature*, vol. 508, pp. 500–503, Apr. 2014.
- [29] J. Kelly, R. Barends, A. Fowler, A. Megrant, E. Jeffrey, T. White, D. Sank, J. Mutus, B. Campbell, Y. Chen, *et al.*, “State preservation by repetitive error detection in a superconducting quantum circuit,” *Nature*, vol. 519, no. 7541, p. 66, 2015.
- [30] J. M. Chow, J. M. Gambetta, E. Magesan, D. W. Abraham, A. W. Cross, B. R. Johnson, N. A. Masluk, C. A. Ryan, J. A. Smolin, S. J. Srinivasan, and M. Steffen, “Implementing a strand of a scalable fault-tolerant quantum computing fabric,” *Nature Communications*, vol. 5, p. ncomms5015, June 2014.
- [31] C. Greganti, M.-C. Roehsner, S. Barz, M. Waegell, and P. Walther, “Practical and efficient experimental characterization of multiqubit stabilizer states,” *Physical Review A*, vol. 91, no. 2, p. 022325, 2015.
- [32] M. Waegell, “Primitive Nonclassical Structures of the  $N$ -qubit Pauli Group,” *Physical Review A*, vol. 89, no. 1, p. 012321, 2014.
- [33] T. C. White, J. Mutus, J. Dressel, J. Kelly, R. Barends, E. Jeffrey, D. Sank, A. Megrant, B. Campbell, Y. Chen, *et al.*, “Preserving entanglement during weak measurement demonstrated with a violation of the bell–leggett–garg inequality,” *npj Quantum Information*, vol. 2, p. 15022, 2016.
- [34] Google Blog: <http://www.googblogs.com/a-preview-of-bristlecone-googles-new-quantum-processor> [Accessed: June 18th, 2018].
- [35] M. Waegell, “Nonclassical structures within the  $n$ -qubit Pauli group,” *arXiv preprint arXiv:1307.6264*, 2013.
- [36] M. Waegell and P. Aravind, “Proofs of the Kochen-Specker theorem based on a system of three qubits,” *Journal of Physics A: Mathematical and Theoretical*, vol. 45, no. 40, p. 405301, 2012.
- [37] M. Waegell and P. Aravind, “Proofs of the Kochen-Specker theorem based on the  $n$ -qubit Pauli group,” *Physical Review A*, vol. 88, no. 1, p. 012102, 2013.
- [38] E. Knill and R. Laflamme, “Theory of quantum error-correcting codes,” *Physical Review A*, vol. 55, no. 2, p. 900, 1997.
- [39] M. A. Nielsen and I. L. Chuang, *Quantum computation and quantum information*. Cambridge University Press, 2010.
- [40] A. Y. Kitaev, “Fault-tolerant quantum computation by anyons,” *Annals of Physics*, vol. 303, no. 1, pp. 2–30, 2003.
- [41] D. P. DiVincenzo and A. Peres, “Quantum code words contradict local realism,” *Physical Review A*, vol. 55, no. 6, p. 4089, 1997.

- [42] D. Collins, N. Gisin, S. Popescu, D. Roberts, and V. Scarani, “Bell-type inequalities to detect true  $n$ -body nonseparability,” *Physical Review Letters*, vol. 88, no. 17, p. 170405, 2002.
- [43] G. Svetlichny, “Distinguishing three-body from two-body nonseparability by a bell-type inequality,” *Physical Review D*, vol. 35, no. 10, p. 3066, 1987.
- [44] M. Seevinck and G. Svetlichny, “Bell-type inequalities for partial separability in  $n$ -particle systems and quantum mechanical violations,” *Physical Review Letters*, vol. 89, no. 6, p. 060401, 2002.
- [45] P. Mitchell, S. Popescu, and D. Roberts, “Conditions for the confirmation of three-particle nonlocality,” *Physical Review A*, vol. 70, no. 6, p. 060101, 2004.
- [46] G. Tóth and O. Gühne, “Detecting genuine multipartite entanglement with two local measurements,” *Physical Review Letters*, vol. 94, no. 6, p. 060501, 2005.
- [47] G. Tóth and O. Gühne, “Entanglement detection in the stabilizer formalism,” *Physical Review A*, vol. 72, no. 2, p. 022340, 2005.
- [48] J. Lavoie, R. Kaltenbaek, and K. J. Resch, “Experimental violation of svetlichny’s inequality,” *New Journal of Physics*, vol. 11, no. 7, p. 073051, 2009.
- [49] M. Waegell, “A bonding model of entanglement for  $n$ -qubit graph states,” *International Journal of Quantum Information*, vol. 12, no. 06, p. 1430005, 2014.

### FIGURES

$\lambda_i$	$O_i$
-1	Y X Y
1	Y Y Z
1	Z X Z
1	Z Y Y

(a)

$\lambda_i$	$O_i$
-1	Z Y X Y
1	Z Y Y Z
1	X Z I I
1	X I X Z
1	I Z Y Y

(b)

$\lambda_i$	$O_i$
1	Z Y Y Z I
1	Z Y X X Y
1	X Z I Z X
-1	X I Y X Y
1	I Z X I X

(c)

$\lambda_i$	$O_i$
1	Z X Z I Z X
-1	Z X I Y X Y
1	X Z Z X Z I
1	X I Y X X Y
1	I Z Y Y I X

(d)

$\lambda_i$	$O_i$
1	Y Y I Y X X Y
1	Y X X Y I X Z
-1	Z Y X X X Y Z
1	Z X Z I I I I
1	I I I I Z Y Y
1	I I Z X Z I I

(e)

$\lambda_i$	$O_i$
-1	Y X Y Z I Z Y Y
1	Y Y I X Z Z Y Y
1	Z X Z Z Y Y Z I
1	Z Y Y I Y Y I X
1	I I Z X I X Z I
1	I I I I Z X I X

(f)

$\lambda_i$	$O_i$
1	Z X Z Z X Z I Z X
1	Z X I Y Y Z Z X Z
1	X Z I Z X I X Z I
1	X I Y Y I X I X Z
-1	I Z Y X Y I X I X
1	I I Z X I X Z I I

(g)

Figure 1. Benchmark IDs for  $N = 3, \dots, 9$  qubits. Each table in (a)–(g) has  $M$  rows of  $N$  observables  $O_{ij}$ , with  $i = 1, \dots, M$  and  $j = 1, \dots, N$ . The product of each row defines  $O_i = \otimes_{j=1}^N O_{ij}$ . Eigenvalues  $\lambda_i$  of  $O_i$  are also shown in each table, chosen to correspond to the state prepared by the circuit of Fig. 2 for the corresponding  $N$ , which lies in the specific eigenspace stabilized by the ID. Combining the rows of each ID with the appropriate eigenvalue defines a correlator observable  $\alpha = \sum_i \lambda_i O_i$ , from which we obtain the experimental benchmark score  $\mathcal{B} = (\langle \alpha \rangle_{\text{exp}} - M + 2)/2$  that witnesses nonlocal  $N$ -partite entanglement when  $0 < \mathcal{B} < 1$ , as well as the lower bound  $F \geq F_{\text{ID}} = (\mathcal{B} + 1)/2$  on the fidelity  $F$  for the state preparation to lie within the indicated eigenspace of the ID.

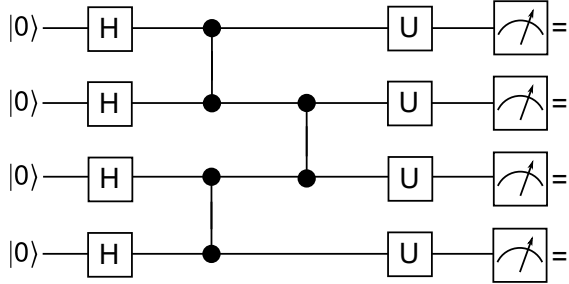
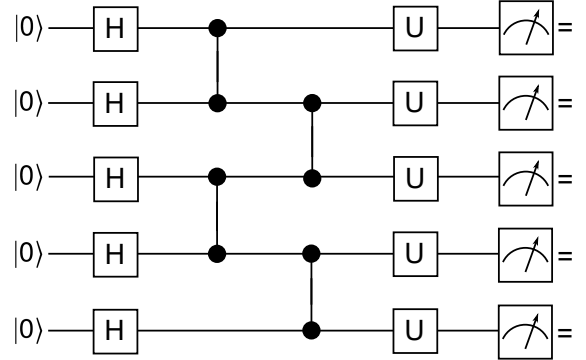
(a)  $N = 4$ (b)  $N = 5$ 

Figure 2. Illustrative circuit diagrams for preparing the states for IDs in Fig. 1, with (a) corresponding to  $N = 4$  in Fig. 1b and (b) corresponding to  $N = 5$  in Fig. 1c. These two examples generalize to  $N$ -qubits, and produce linear cluster states. The local measurement settings for each observable  $O_{ij}$  in the ID are implemented by the unitary operations  $U_{ij}$ , assuming detectors that naturally measure the  $Z$  basis. This circuit allows the  $M$  different settings of an ID to be implemented with different  $U_{ij}$  for different observables and qubits. For example, in the 5-qubit ID of Fig. 1c the first setting is  $ZYYZI$ , meaning that for the first and fourth qubits  $U_{11} = U_{14} = I$ , for the second and third qubits  $U_{12} = U_{13} = e^{i\pi X/4}$ , and the fifth qubit is ignored.

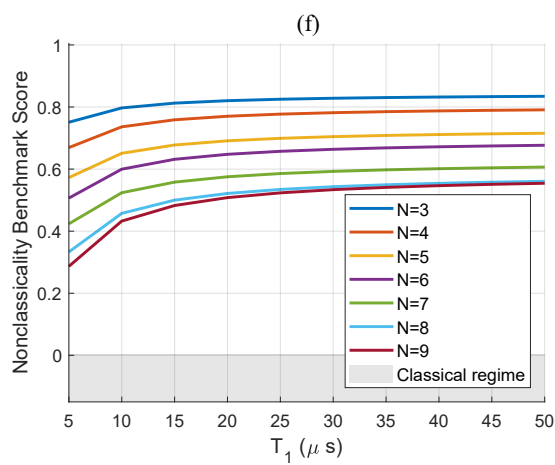
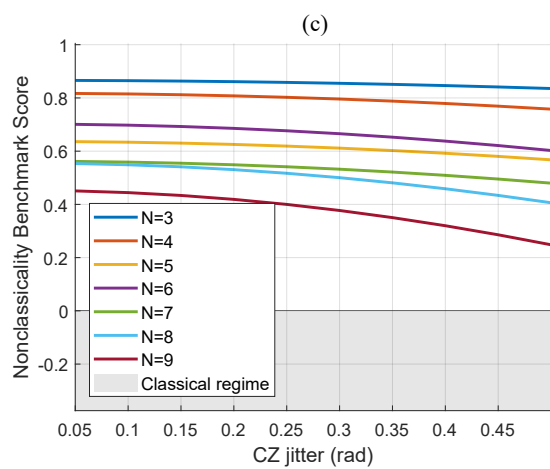
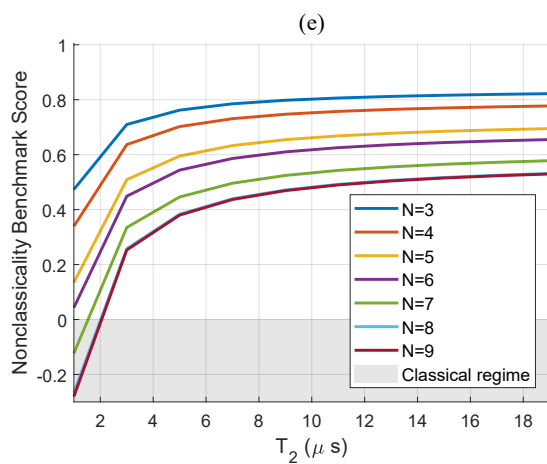
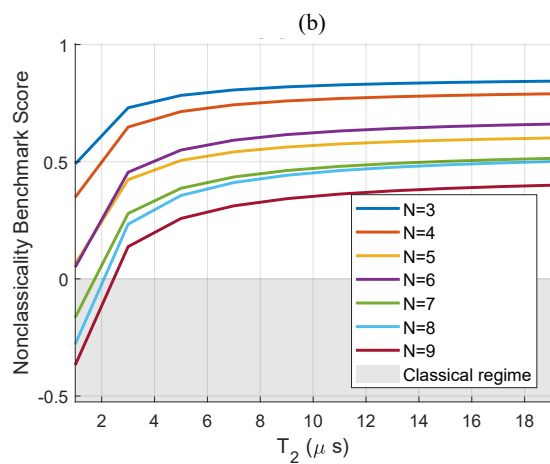
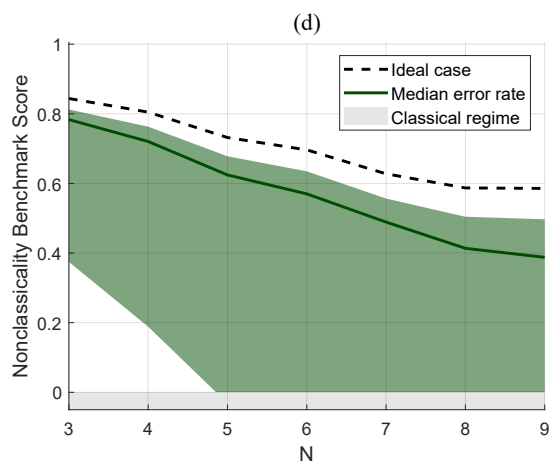
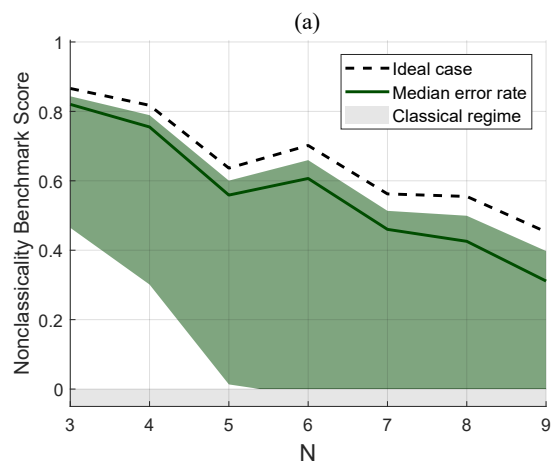


Figure 3. Nonclassicality Benchmark Scores ( $\mathcal{B}$ ), for selected simulations. The nonideality parameter ranges were  $T_1 \in [5, 50] \mu\text{s}$  energy relaxation times,  $T_2 \in [1, 19] \mu\text{s}$  dephasing times, and  $w \in [0.05, 0.5]$  rad of angular jitter widths for  $ZZ_{90}$  decompositions of controlled- $Z$  (CZ) gates. We used a single-qubit gate time of  $\Delta t = 25$  ns, and a 2-qubit controlled- $Z$  gate time of  $\Delta t = 45$  ns, which are conservative estimates for the reported gate times. In plots (e) and (f), the curves for qubit numbers  $N = 3, \dots, 9$  are ordered starting from the top curve. In plots (b) and (c), the  $N = 5$  lines are below the  $N = 6$  lines, and the  $N = 7$  lines are below the  $N = 8$  lines, due to the poor performance of chip qubits 5 and 7 (boldface values). (a,b,c) Simulated data using Google’s 9-qubit-chip values [28, 29]:  $\{T_1\} = \{18.6, 28.1, 22.0, 19.1, \mathbf{41.1}, 21.3, \mathbf{39.2}, 24.7, 26.3\} \mu\text{s}$  and  $\{P_e\} = \{1.8, 1.1, 1.7, 1.3, \mathbf{4.8}, 0.7, \mathbf{6.7}, 0.4, 1.5\} \%$ . (d,e,f) Simulated data for  $P_e = 2\%$  initialization error, with parameter ranges centered on mean chip values. (a,d)  $\mathcal{B}$  vs.  $N$ . Ideal curves have  $T_2 = T_1 = \infty$  and  $w = 0$ . Median curves approximate the chip, with shading indicating the range of simulated values. (b,e)  $\mathcal{B}$  vs.  $T_2$ , fixing median chip values of  $w$  and  $T_1$ . (c)  $\mathcal{B}$  vs.  $w$ , fixing the median chip value of  $T_2$ . (f)  $\mathcal{B}$  vs.  $T_1$ , fixing the median chip values of  $T_2$  and  $w$ .

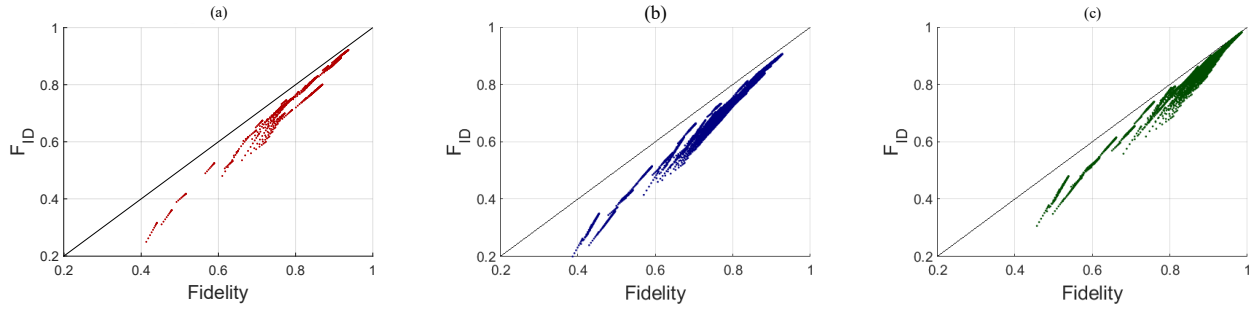


Figure 4. Scatterplots of the fidelity lower bound  $F_{ID}$  vs. true fidelity  $F$  for all simulated data. The lower bound is reasonably tight for all data, and when  $F \rightarrow 1$  so too does  $F_{ID}$ . All plots contain data for the nonideality ranges:  $T_2 \in [1, 19] \mu\text{s}$  dephasing times, and  $w \in [0.05, 0.5]$  rad angular jitter widths for CZ gates. (a) Chip values  $\{T_1\} = \{18.6, 28.1, 22.0, 19.1, \mathbf{41.1}, 21.3, \mathbf{39.2}, 24.7, 26.3\} \mu\text{s}$  energy relaxation times, and  $\{P_e\} = \{1.8, 1.1, 1.7, 1.3, \mathbf{4.8}, 0.7, \mathbf{6.7}, 0.4, 1.5\} \%$  initialization error. (b)  $P_e = 2\%$  initialization error, with range  $T_1 \in [5, 50] \mu\text{s}$ . (c) Same ranges as the center plot, but with  $P_e = 0$  to show the asymptotic approach  $F_{ID} \rightarrow F$  as  $F \rightarrow 1$ .